

The Estimation of Black-Hole Masses in Distant Radio Galaxies

M.L. Khabibullina^a, O.V. Verkhodanov^a

^aSpecial Astrophysical Observatory of the Russian AS, Nizhnij Arkhyz 369167, Russia

Received 2010; accepted October 22, 2010.

We have estimated the masses of the central supermassive black holes of 2442 radio galaxies from a catalog compiled using data from the NED, SDSS, and CATS databases. Mass estimates based on optical photometry and radio data are compared. Relationships between the mass of the central black hole M_p^{bh} and the redshift z_p are constructed for both wavelength ranges. The distribution of the galaxies in these diagrams and systematic effects influencing estimation of the black-hole parameters are discussed. Upper-envelope cubic regression fits are obtained using the maximum estimates of the black-hole masses. The optical and radio upper envelopes show similar behavior, and have very similar peaks in position, $z_p \simeq 1.9$ and amplitude, $\log M_p^{bh} = 9.4$. This is consistent with a model in which the growth of the supermassive black holes is self-regulating, with this redshift corresponding to the epoch when the accretion-flow phase begins to end and the nuclear activity falls off.

PACS: 98.54.-h, 98.54.Gr, 98.62.Ve, 98.70.Dk, 98.80.Es

1. INTRODUCTION

One of the central questions in studies of distant radio galaxies (redshifts $z > 0.3$) is the origin and growth rate of supermassive black holes (SMBHs) in their nuclei. The discovery of radio galaxies and quasars at high redshifts has raised the need to explain the rapid formation of SMBHs in early epochs of the evolution of the Universe. For example, radio galaxies have been detected at $z = 5.19$ (TN J0924-2201) [1], when the age of the Universe was only $t \sim 1.1 \times 10^9$ yrs (in a cosmology with $\Omega_m = 0.27$, $\Omega_\Lambda = 0.73$, $H_0 = 70$ km s⁻¹Mpc⁻¹), and $z = 4.515$ [2], when $t \sim 1.3 \times 10^9$ yrs. Quasars have been found in the Sloan Digital Sky Survey (SDSS) at redshifts of $z = 6.42$ (J114816.64+525150.3), $z = 6.23$ (J104845.05+463718.3), and $z = 6.05$ (J163033.90+401209.6) [3], when the age of the Universe was $t \sim 850$ -900 million years. Willot et al. [4] used the width of the emission lines of the quasar J114816.64+525150.3 at $z = 6.42$ to estimate the mass of its SMBH to be $M_{bh} = 3 \times 10^9 M_\odot$. The rapid (over 800 million years) formation of SMBHs in a Λ CDM cosmology requires special models for their growth rates. As was noted by Loeb [5], if the formation of massive black holes is described by a hierarchical scheme similar to that for the formation of their parent galaxies, this process must be rapid and efficient. Models with primordial massive black

holes that formed after the Big Bang but before the formation of galaxies are often invoked to explain the early existence of SMBHs.

It is believed that SMBHs play a central role in the formation and evolution of massive galaxies, and are also a key component in the development of nuclear activity. However, it remains unclear how galaxies and their central SMBHs are related to the formation of observed structures [6]-[8]. An important result obtained from measurements of black-hole masses in nearby galaxies is the existence of an appreciable correlation between the mass of the central black hole and the mass of the bulge of the host galaxy, which gives rise to correlations between the black-hole mass and the luminosity of the bulge [9],[10] and between the black-hole mass and the stellar velocity dispersion σ (e.g. [11]-[16]). This result is based on a small number of nearby galaxies for which direct black-hole mass measurements are available (~ 30), and there is appreciable scatter in the relation (~ 0.4 in the logarithm of the black-hole mass). Nevertheless, these empirical relations provide a new tool for estimating black-hole masses in various types of active galactic nuclei (AGNs), when the bulge luminosity and/or stellar-velocity distribution is known [17]-[19]. The existence of these correlations can provide constraints on the evolution of AGNs, and can be used to test whether AGNs precisely follow these relations or not.

Franceschini et al. [20] established the existence of a correlation between the radio power of AGNs and the masses of their black holes. A number of studies have also demonstrated relationships between black-hole masses and radio powers for samples of nearby galaxies, but these results differ from one another [21]-[24]. Discussions of this relation were also extended to more active galaxies, such as Seyfert galaxies and quasars (see, for example, [23],[25]-[28]).

A number of studies have used data from the SDSS [29] for quasars to estimate the growth rates of their SMBHs. Kelly et al. [30] constructed the black-hole mass function for a sample of 9886 broadline quasars with redshifts $1 < z < 4.5$. Their results support the "downsizing" effect for black holes in broad-line quasars, whose peak number density shifts toward high z as the black-hole mass is increased¹. This peak occurs at $z \sim 2$. Moreover, Kelly et al. [30] estimated the completeness of the SDSS sample as a function of black-hole mass and the ratio of the luminosity of a quasar to the Eddington luminosity, L/L_{Edd} , and found that the sample of black-hole masses $\leq 10^9 M_\odot$ and $L/L_{Edd} \leq 0.5$ is very incomplete at redshifts $z < 1$. According to their model, they estimate the lifetime of the broad-line quasar stage to be approximately 150 million years at $z = 1$ for a black-hole mass of $\sim 10^9 M_\odot$. Shen et al. [31] constructed a sample of 105783 quasars based on the SDSS, and used various properties (emission in $H\alpha$, $H\beta$, $MgII$, CIV ; radio data; broad absorption lines) to estimate their black-hole masses. They also obtained a logarithmic dependence between the black-hole masses and the luminosities and widths of the lines used.

Here, we verify two dependences of the black-hole masses on the radio and optical luminosities that are used in the literature in studies of radio galaxies. We used data from the SDSS, NED, and CATS databases to construct a sample of distant ($z < 0.3$) radio galaxies, for which we derived and compared these dependences for the black-hole mass. We calculated the luminosities using optical data in the R filter and 5-GHz radio flux densities. We assumed a Λ CDM cosmology with $H_0 = 71 \text{ km s}^{-1} \text{ Mpc}^{-1}$, $\Omega_M = 0.27$, and $\Omega_\Lambda = 0.73$. We used a catalog of distant radio galaxies with spectroscopic redshifts $z < 0.3$, which were selected based on data from the largest available databases [32]-[35].

2. STUDIED SAMPLE AND MASS ESTIMATES

2.1. Input Data

A sample of radio galaxies with $z < 0.3$ [32]-[35] was constructed using the NED (<http://nedwww.ipac.caltech.edu>), CATS (<http://cats.sao.ru>) [36],[37], and SDSS (<http://www.sdss.org>) [28] databases. This sample can be used to carry out various statistical and cosmological tests requiring a comparatively large number of objects of a single type [37]-[39]. The NED database was used to construct the initial list of sources, selecting objects with specified parameters, most importantly with redshifts $z < 0.3$ and morphologies corresponding to radio galaxies. The initial catalog contained 3364 objects. This galaxy sample was contaminated by objects with incomplete information and objects with other properties. Therefore, we paid special attention to eliminating unwanted sources from the initial sample, including (1) galaxies with redshifts determined using photometric methods and (2) galaxies with quasar-like properties according to data from the literature. The final catalog contains 2442 sources with spectroscopic redshifts, photometric data and radio flux densities, radio sizes, and radio spectral indices, calculated via cross identification with other radio catalogs in the CATS database at frequencies from 30 GHz to 325 MHz.

2.2. Estimating the SMBH Masses. Optical Data

To estimate the SMBH masses, we used the relationship between the black-hole masses and R absolute magnitudes ($M_{bh} - M_R$) from [16], which was obtained via an analysis of the magnitudes and stellar velocities in AGNs:

$$\log\left(\frac{M_{bh}}{M_\odot}\right) = -0.50(\pm 0.02)M_R - 2.27(\pm 0.48),$$

where M_R is the absolute R magnitude of the bulge, assuming that the bulge of an elliptical galaxy essentially represents the entire galaxy.

Since R observations are not available for all the catalog radio galaxies, we estimated the R luminosities of a number of objects based on data in other filters using the database of galactic spectral-energy distributions (SEDs) [40]. Photometric data were used to estimate the ages of the radio galaxies, assuming that their SEDs corresponded to the SEDs of elliptical galaxies. We determined the R magnitude using the redshift and the age of the corresponding model SED track. We used the GISSEL model data [41],

¹ The "Downsizing" scenario, which can explain a mass dependence of the evolutionary history in which less massive elliptical galaxies have longer star-formation histories than more massive elliptical galaxies.

which contains synthetic spectra of elliptical galaxies for ages from 200 million years to 14 billion years, as the basic library of tracks. This library can be accessed both in the HyperZ package [42] and at the site <http://sed.sao.ru> [40]. The distribution of estimated and measured R magnitudes for the radio-galaxy sample is shown in Fig. 1.

The luminosity was calculated using the formula [43] (see also [44])

$$L = 4\pi F d_L^2(z),$$

where F is the measured flux, $d_L(z) = (1+z) \int_0^z \frac{dz'}{H(z')}$, is the luminosity distance, and $H(z) = H_0[\Omega_R(1+z)^4 + \Omega_m(1+z)^3 - (\Omega_0 - 1)(1+z)^2 + \Omega_\Lambda]^{1/2}$ is the Hubble parameter. The resulting luminosity (more precisely, absolute magnitude) was used to estimate the masses of the central black holes of the galaxies. The distribution of estimated black-hole masses is shown in Fig. 1.

2.3. Estimating the SMBH Masses. Radio Data

To calculate the estimated black-hole masses based on radio data, we used the relationship between the radio luminosity and black-hole mass ($P_{5\text{GHz}} - M_{bh}$) from [20]:

$$P_{5\text{GHz}} \propto \left(\frac{M_{bh}}{M_\odot}\right)^{2.2 \div 3.0},$$

where $P_{5\text{GHz}}$ is the total power at 5 GHz. Our calculations used the formula

$$P_{5\text{GHz}} \propto \left(\frac{M_{bh}}{M_\odot}\right)^{3.0}.$$

We calculated the radio power using the standard formula [43]

$$P_\nu = 4\pi d_L^2 S\left(\frac{\nu}{(1+z)}\right)(1+z)^{-1},$$

where $S\left(\frac{\nu}{(1+z)}\right)$ is the source flux density at frequency ν taking into account the redshift and d_L is the photometric distance. The value $S\left(\frac{\nu}{(1+z)}\right)$ was determined from the continuum radio spectrum of each source, constructed via fitting with a standard set of functions. We used the spg program [45] of the RATAN-600 continuum data-reduction system for this purpose. For radio galaxies with measurements at only one frequency, we took the spectral index to be equal to the median value for our sample [32] at 1.4 GHz ($\alpha_{med} = -0.63$). The distribution of the obtained radio power at 5 GHz is shown in Fig. 2.

3. DISCUSSION

A comparison of the masses estimated using radio and optical data shows a clear difference in the shapes of the mass distributions (Figs. 1 and 2). Moreover, in contrast to the distribution of optical mass estimates, the distribution of radio mass estimates is two-peaked. This could result from evolutionary manifestations in the radio flux at different redshifts at which the radio sources are ignited and then quiet down. Then, we may obtain different estimates for the mass of the "central engine" based on the radio flux, corresponding to different stages of activity. The higher peak in the distribution in Fig. 2 corresponds to closer objects with lower masses, observed in the SDSS. Note that, in spite of the two-peaked form of the mass distribution, the radio data provide a smaller scatter in the redshift distribution (Fig. 3). We should note that nonlinearity of "radio luminosity — optical luminosity" relation having the underlying relation of radio luminosity and black hole mass was demonstrated in 1960-s by Pskovskii [46] and corrected by Iskudarian and Pariiskii [47].

While the optical black-hole mass estimates can tentatively be divided into two subgroups—strongly clustered at $z \lesssim 0.7$ and weakly clustered at $z \gtrsim 0.7$ —this is not the case for the radio mass estimates. The range of black-hole masses derived using the radio data is two orders of magnitude smaller than that for the optically derived masses. The mean radio masses in individual redshift intervals ($\Delta z = 0.5$) are higher than the corresponding optical masses. Although the radio estimates also display clustering at $z \lesssim 0.7$ for the first subsample, the objects of the second subsample are grouped along the line for the median regression fit.

Figure 3 shows the least-squares regression fits and upper envelopes for both types of data. For the optical data (Fig. 3, left), the fit for the median values on the log MRbh- z diagram² in bins $\Delta z = 0.5$ yields a growing function satisfying the linear relation $\log M_R^{bh} = 0.387(\pm 0.134) \cdot z + 7.665(\pm 0.309)$, where M_R^{bh} is the black-hole mass estimated using the R optical data. The upper envelope is described by a cubic function: $\log M_R^{bh} = 9.058 + 0.783 \cdot z - 0.303 \cdot z^2 + 0.030 \cdot z^3$. Similarly, the linear fit for the radio data (Fig. 3, right) has the form $\log M_{rad}^{bh} = 0.126(\pm 0.027) \cdot z + 8.793(\pm 0.073)$, the upper envelope the form $\log M_{rad}^{bh} = 9.084 + 0.347 \cdot z - 0.120 \cdot z^2 + 0.011 \cdot z^3$. In spite of the difference in the dispersion of the mass estimates, the positions and amplitudes of the maxima of both upper envelopes are similar:

² Here and below, the black-hole masses are expressed in solar masses, M_\odot

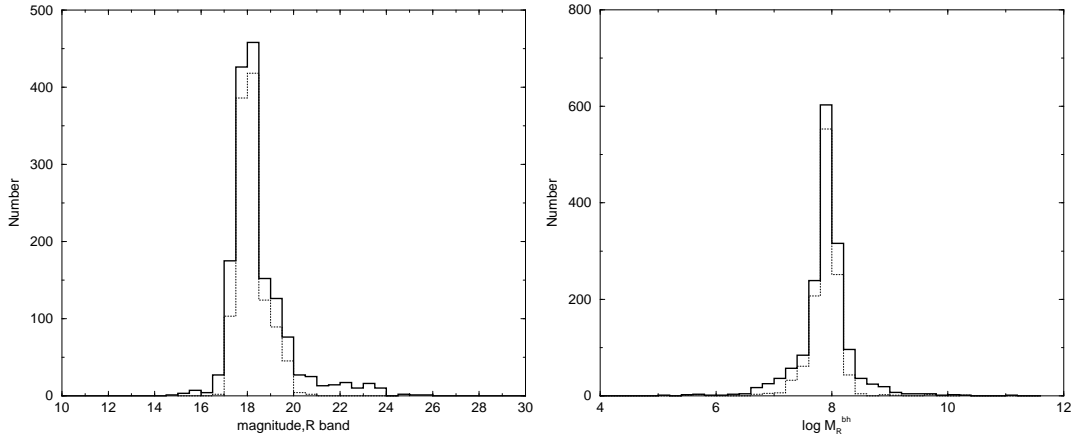


Figure 1: *Left: distribution of R magnitudes for the sample of radio galaxies. Right: distribution of black-hole masses obtained from R data for the sample of radio galaxies. The SDSS subsample of radio galaxies is shown by the dotted line.*

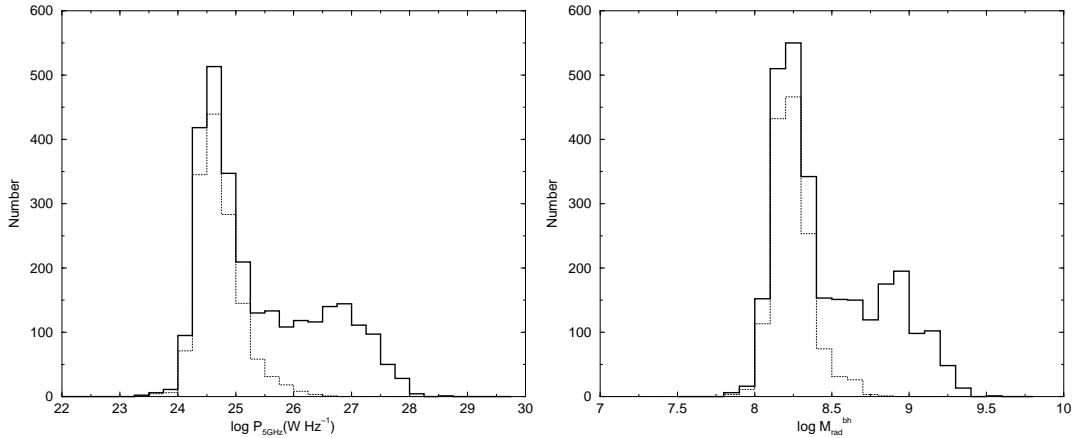


Figure 2: *Left: distribution of the 5-GHz radio power for the radio-galaxy sample. Right: distribution of the black-hole masses obtained from the total radio power (luminosity) at 5 GHz. The SDSS subsample of radio galaxies is shown by the dotted line.*

the peak is at $z_p = 1.78$ and $\log M_p^{bh} = 9.67$ for the optical data, and at $z_p = 1.92$ and $\log M_p^{bh} = 9.38$ for the radio data.

The location of the maxima in the redshift range $1.5 \lesssim z \lesssim 2$ (with similar values for both the optical and radio estimates) could be associated with some sort of systematic effect reflecting real physical processes. This range of z corresponds to an epoch of massive “ignition” of radio sources as a result of mergers between galaxies in galaxy clusters. In this case, due to selection effects, we will most likely detect objects with the maximum luminosity, which means those with the maximum estimated black-hole masses, in this range.

Note that this result obtained for our list of radio galaxies is consistent with the results of [30], where a

sample of broad-line quasars from the SDSS was considered. Kelly et al. [30] found that the peak number density of SMBHs in broad-line quasars occurs at $z \sim 2$. The location of the mass-distribution peak at $z \sim 2$ is consistent with a self-regulating growth model for the SMBHs, with this being the epoch when the end of the accretion-flow phase begins and the nuclear activity starts to fall off. Note that our estimates and the estimate of [30] are also consistent with self-regulation of the rate of formation of galaxies in halos of dark matter via the interaction of the jets from the central object with the intergalactic gas [48].

A growth in the black-hole mass with increasing redshift is visible in both diagrams, demonstrated by the linear fits. The uncertainties in the fit parameters characterize the statistical scatter in the masses

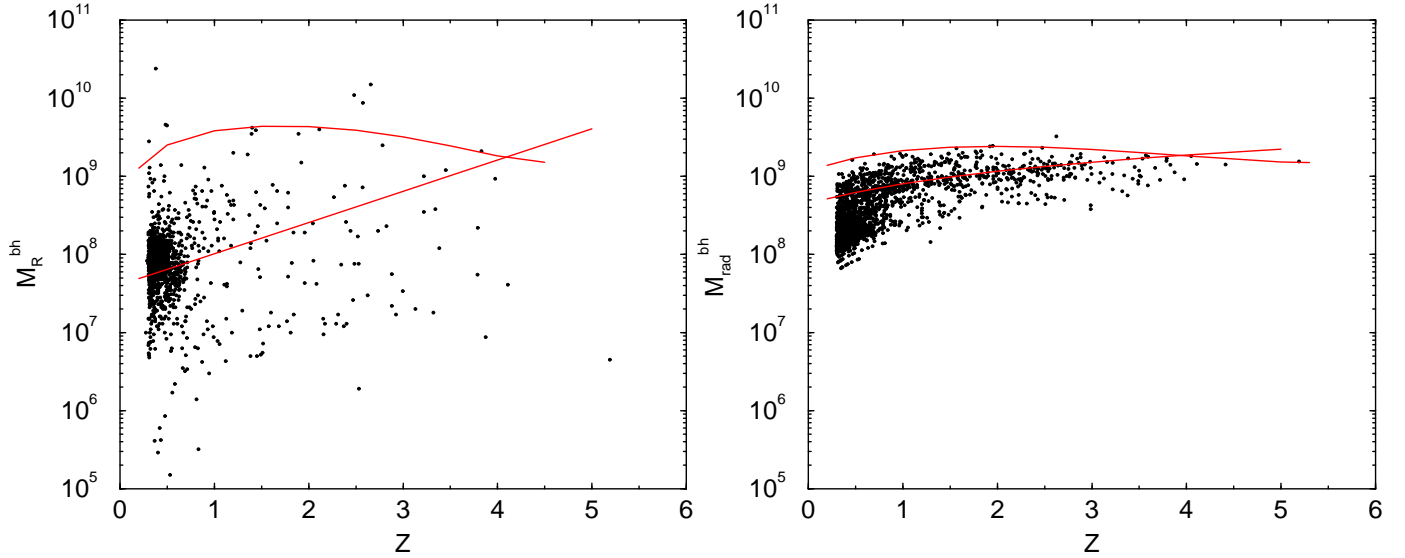


Figure 3: *Plots of black-hole mass versus redshift for the radio galaxies, based on R optical data (left) and 5-GHz radio data (right). Regression fits were constructed for the mean and maximum black-hole masses in intervals $\Delta z = 0.5$.*

(and luminosities) derived using the optical and radio data. The large scatter for the optical estimates, in particular the many deviations from the maximum values, indicates small ratios of the optical to the Eddington luminosities, and may suggest that some Seyfert 2 galaxies have been included in our sample. The linear fit based on the median masses may reflect selection effects in the detection of distant objects, and the region of intersection with the upper envelope ($z_c = 4.14, \log(M_c) = 9.27$ for the optical and $z_c = 3.57, \log(M_c) = 9.25$ for the radio) shows an upper limit, beyond which this effect will dominate. Note, however, that only a few radio galaxies have been detected in this region [2].

The $M_{opt}^{bh} - M_{rad}^{bh}$ relation indicates the region in which the two methods used to estimate the masses of the SMBHs are statistically applicable, and shows the amount of scatter obtained using these methods (Fig. 4). Three regions of clustering can be distinguished on this plot, for two of which we obtained fits in the form $\log M_R^{bh} = a \cdot \log M_{rad}^{bh} + b$. The parameters for the first group of clustered points are $a = -0.036 \pm 0.026$, $b = 8.122 \pm 0.219$, and those for the second group of points $a = 1.211 \pm 0.029$, $b = -2.329 \pm 0.261$. The data for radio galaxies from different redshift ranges are shown by different symbols: $0.3 \leq z < 0.7$ (points), $0.7 \leq z < 1.5$ (crosses), and $1.5 \leq z$ (triangles). The high concentration of points in the left part of the diagram is due to the large number of comparatively nearby radio galaxies in the SDSS, for which relatively similar black-hole

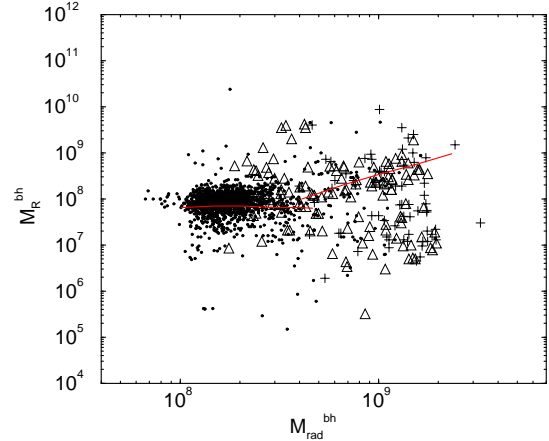


Figure 4: *Plot of M_{opt}^{bh} versus M_{rad}^{bh} for R-band and 5-GHz data. Regression fits were obtained for two regions where the points are concentrated. Data for radio galaxies from different redshift ranges are denoted with different symbols: $0.3 \leq z < 0.7$ (points), $0.7 \leq z < 1.5$ (crosses), and $1.5 \leq z$ (triangles).*

masses were obtained.

Figure 4, and also Figure 1, show that the mean estimated masses for the "central engines" for the SDSS subsample of galaxies are $\sim 10^8 M_\odot$ based on the optical data and from 10^8 to $10^9 M_\odot$ based on the radio data. In general, nearly all the radio galaxies in the sample have $M_{opt}^{bh} \leq M_{rad}^{bh}$. For a second group, many of which are distant radio galaxies with $z \geq 1.5$ we observe a correlation between the two mass esti-

mates for the central objects. The objects in the lower right part of Fig. 4 have low optical and high radio mass estimates. These low estimates from the region of the lower envelope on the left $M_{bh}(z)$ diagram in Fig. 3 and the corresponding estimates in the right diagram may be associated with non-elliptical subclasses of radio galaxies.

We can distinguish several selection effects that are inevitable when estimating the central black-hole masses, even when care is taken in selecting galaxies according to their optical and radio properties. Their manifestation can explain differences between results obtained using different methods to determine the central black-hole masses. These selection effects include the following:

1) more distant objects tend to be more powerful; i.e., a sample of distant objects contains, on average, galaxies with higher black-hole masses;

2) although the sample has been cleaned of objects with the properties of quasars (such as broad $H\alpha$ emission), some such objects with relatively weak lines may remain in the subsample of comparatively nearby ($z \lesssim 0.7$) sources;

3) the SDSS objects in our catalog should not include Seyfert 2 galaxies with narrow lines; in spite of their radio emission, these galaxies have low ratios of their bolometric to Eddington luminosities (see, e.g., [49]), and their luminosities should thus place them in the lower part of the diagram (Fig. 2);

4) the presence of evolutionary effects that are strongly manifest in the radio, such as the fact that some radio galaxies may be observed in early phases of their activity, and that galaxies with central black holes of the same mass may have radio fluxes differing by an order of magnitude;

5) some comparatively nearby objects whose peak activity in the radio has passed have black-hole mass estimates derived from velocity dispersions calibrated based on the radio fluxes; in this case, the use of dependences for more distant galaxies can lead to overestimation of the black-hole masses.

Nevertheless, the similarity of the behaviors of the mass upper envelopes (Fig. 3) suggests that these estimates are trustworthy for objects with the highest luminosities (close to the Eddington values). The comparatively small scatter of the radio masses for various z makes it possible to use this diagram to estimate masses with a mean accuracy of less than an order of magnitude, or even half an order of magnitude at $z \lesssim 1.5$. This is confirmed by the plot in Fig. 4, where a correlation between the radio and optical masses is observed for most radio galaxies with $z \lesssim 1.5$.

We used the other parameters in our catalog to construct plots of the black-hole mass versus radio

spectral index (Fig. 5) and versus the apparent size of the radio source (Fig. 6) for a single type of galaxies with active nuclei (i.e., radio galaxies). The former plot shows a correlation between the radio mass estimates and the radio spectral index

$$\alpha = 2.73(\pm 1.56) - 0.18(\pm 0.08) \cdot \log(M_{bh}),$$

There is a tendency for more powerful radio galaxies, which presumably have higher nuclear activity, and possibly higher masses for their central engines, to have steeper spectra (i.e., smaller spectral indices). Of course, it cannot be ruled out that some selection effect is hidden via the redshift dependence of the spectral index $\alpha(z)$ found in [35]. Distant radio galaxies are often selected in surveys based on their spectral indices, and distant sources tend to be more powerful; therefore, this effect should make some contribution to the detected dependence. However, the physical properties of the objects themselves at various z probably dominate in the $\alpha(z)$ relation.

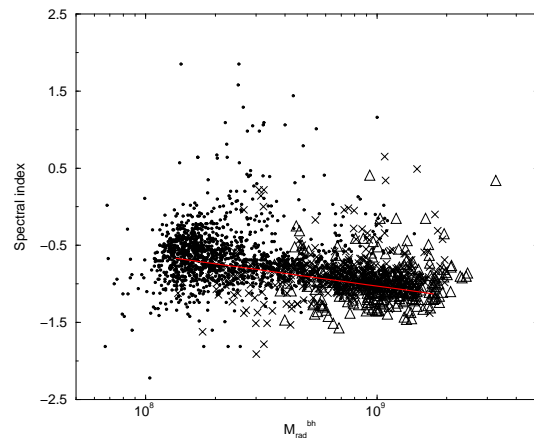


Figure 5: Plot of black-hole mass versus radio spectral index. The masses were estimated using the radio data. Notation is the same as in Fig. 4.

Figure 6 shows the distribution of the angular sizes of radio galaxies according to the NVSS data [50] as a function of their radio black-hole mass estimates. Most of the objects distributed along the horizontal axis have small angular sizes ($\lesssim 25''$), determined by the resolution of the NVSS ($\sim 45''$), and most of these are SDSS objects with redshifts $z \lesssim 0.7$. Note that the central objects of the most extended objects ($\gtrsim 1'$) cover the entire range of masses, and are encountered in all three redshift intervals we have considered.

4. CONCLUSION

We have carried out a comparative analysis of estimates of the central black-hole masses of 2442 radio

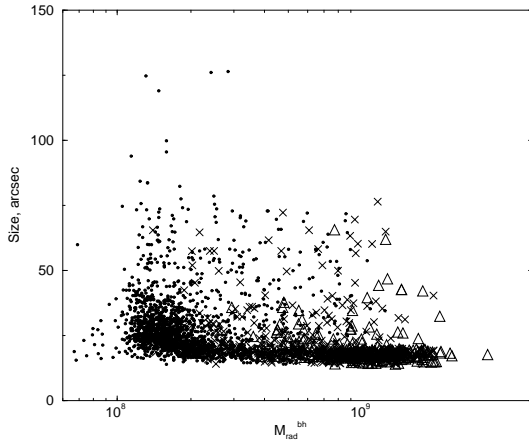


Figure 6: *Masses estimated using the radio data. The apparent sizes of the galaxies were taken from the NVSS catalog [48]. Notation is the same as in Fig. 4.*

galaxies with $z \lesssim 0.3$ [32]–[34], derived from relations between the black-hole mass and the R luminosity [17] and between the black-hole mass and the radio power [20]. Appreciable differences between these two estimates are observed for many of the radio galaxies. We have discussed various systematic effects associated with observational selection effects and the evolutionary properties of the radio galaxies that could lead to these differences. However, a diagram of M_R^{bh} versus M_{rad}^{bh} (Fig. 4) reveals a region where these two mass estimates are correlated. This zone is formed primarily by the distant radio galaxies in our sample. Moreover, the upper envelopes constructed using the maxima of the two mass estimates (Fig. 3) show similar behavior and have very similar positions ($z_p \simeq 1.9$) and amplitudes ($\log M_p^{bh} = 9.4$). This is consistent with self-regulation of the growth of the central SMBH, when the end of the accretion flow begins and the activity of the galactic nucleus falls off. The $M_{rad}^{bh}(z)$ diagram displays comparatively narrow scatter, and should be preferred for use in estimating galactic black-hole masses.

ACKNOWLEDGMENTS

This research has made use of the NASA/IPAC Extragalactic Database (NED), which is operated by the Jet Propulsion Laboratory, California Institute of Technology, under contract with the National Aeronautics and Space Administration. We have also used the CATS database of radio astronomy catalogs [36] and the FADPS system for radio astronomical data reduction (http://sed.sao.ru/~vo/fadps_e.html) [51],[52]. We are deeply grateful to R.D. Dagkesamanskii for valuable comments on the manuscript. This work was supported by the Program of State Support for Leading Scientific Schools of the Russian Federation (School of S.M. Khaikin) and the

Russian Foundation for Basic Research (projects 09-02-00298, 09-02-92659-IND, 08-02-00486). OVV also thanks the "Dinasty" Funding for Non-commercial Programmes for partial support.

References

- M. van Breugel, C. de Breuck, S.A. Stanford, et al., *Astrophys. J.* **518**, 61 (1999); arXiv:astro-ph/9904272 (1999).
- A.I. Kopylov, W.M. Goss, Yu.N. Pariiskii, et al., *Pis'ma Astron. Zh.* **32**, 483 (2006) [*Astron. Lett.* **32**, 433 (2006)]; arXiv:0705.2771 [astro-ph] (2007).
- X. Fan, M.A. Strauss, R.H. Becker, et al., *Astron. J.* **132**, 117 (2006); arXiv:astro-ph/0512082 (2005).
- C.J. Willot, R.J. McLure, and M.J. Jarvis, *Astro-phys. J.* **587**, L1 (2003).
- A. Loeb, *Astrophys. J.* **403**, 542 (1993).
- J. Silk and M.J. Rees, *Astron. Astrophys.* **331**, L1 (1998).
- M.G. Haehnel and G. Kau mann, *Mon. Not. R. Astron. Soc.* **318**, L35 (2000).
- F.C. Adams, D.S. Gra , and D.O. Richstone, *Astrophys. J.* **551**, L31 (2001).
- J. Magorian et al., *Astron. J.* **115**, 2285 (1998).
- J. Kormendy and K. Gebhardt, *AIP Conf. Proc.* **586**, 363 (2001).
- L. Ferrarese and D. Merritt, *Astrophys. J.* **539**, L9 (2000).
- K. Gebhardt, R. Bender, G. Bower, et al., *Astrophys. J.* **539**, L13 (2000).
- S. Tremaine, K. Gebhardt, R. Bender, et al., *Astrophys. J.* **574**, 740 (2002).
- T.R. Lauer, S.M. Faber, D. Richstone, et al., *Astrophys. J.* **662**, 808 (2007).
- Wei-Hao Bian, Yan-Mei Chen, Chen Hu, et al., *Chin. J. Astron. Astrophys.* **8**, 522 (2008).
- J. Kormendy and R. Bender, *Astrophys. J.* **691**, 142 (2009).
- R.J. McLure and J.S. Dunlop, *Mon. Not. R. Astron. Soc.* **331**, 795 (2002).
- R. Falomo, N. Carangelo, and A. Treves, *Mon. Not. R. Astron. Soc.* **343**, 505 (2003).
- D. Betton et al., *Astron. Astrophys.* **399**, 869 (2003).
- A. Franceschini, S. Vercellone, and A.C. Fabian, *Mon. Not. R. Astron. Soc.* **297**, 817 (1998).
- I. Yi and S.P. Boughn, *Astrophys. J.* **515**, 576 (1999).
- P. Salucci, E. Szuszkiewicz, P. Monaco, and L. Danese, *Mon. Not. R. Astron. Soc.* **307**, 637 (1999).
- A. Laor, *Astrophys. J.* **543**, 111 (2000).
- T. Di Matteo, C.L. Carilli, and A.C. Fabian, *Astrophys. J.* **547**, 731 (2001).
- C.H. Nelson, *Astrophys. J.* **544**, 91 (2000).
- R.J. McLure and J.S. Dunlop, *Mon. Not. R. Astron. Soc.* **327**, 199 (2001).
- M. Lacy, S.A. Laurent-Muehleisen, S.E. Ridgway, et al., *Astrophys. J.* **551**, 17 (2001).
- M. Gu, X. Cao, and D.R. Jiang, *Mon. Not. R. Astron. Soc.* **327**, 1111 (2001).
- D.P. Schneider, P.B. Hall, G.T. Richards, et al., *Astron. J.* **134**, 102 (2007).

- B.C. Kelly, M. Vestergaard, Xi. Fan, et al., arXiv:1006.3561 [astro-ph] (2010).
- Y. Shen, P.B. Hall, G.T. Richards, et al., arXiv:1006.5178 [astro-ph] (2010).
- M.L. Khabibullina and O.V. Verkhodanov, *Astrophys. Bull.* **64**, 123 (2009); arXiv:0911.3741 [astro-ph] (2009).
- M.L. Khabibullina and O.V. Verkhodanov, *Astrophys. Bull.* **64**, 276 (2009); arXiv:0911.3747 [astro-ph] (2009).
- M.L. Khabibullina and O.V. Verkhodanov, *Astrophys. Bull.* **64**, 340 (2009); arXiv:0911.3752 [astro-ph] (2009).
- O.V. Verkhodanov and M.L. Khabibullina, *Pis'ma Astron. Zh.* **36**, 9 (2010) [*Astron. Lett.* **36**, 7 (2010)].
- O.V. Verkhodanov, S.A. Trushkin, H. Andernach, and V.N. Chernenkov, *Bull. Spec. Astrophys. Observ.* **58**, 118 (2005); arXiv:0705.2959 [astro-ph] (2007).
- O.V. Verkhodanov, S.A. Trushkin, H. Andernach, and V.N. Chernenkov, *Data Sci. J.* **8**, 34 (2009); arXiv:0901.3118 [astro-ph] (2009).
- O.V. Verkhodanov and Yu.N. Pariiskii, *Bull. Spec. Astrophys. Observ.* **55**, 66 (2003).
- O.V. Verkhodanov and Yu.N. Pariiskii, *Radio Galaxies and Cosmology* Fizmatlit, Moscow, 2009) [in Russian].
- O.V. Verkhodanov, A.I. Kopylov, O.P. Zhelenkova, et al., *Astron. Astrophys. Trans.* **19**, 663 (2000); arXiv:astro-ph/9912359 (1999).
- G. Bruzual and S. Charlot, *Astrophys. J.* **405**, 538 (1993).
- M. Bolzonella, J.-M. Miralles, and R. Pello, *Astron. Astrophys.* **363**, 476 (2000).
- C. Lang, *Astrophysical Formulae* (Springer, New York, 1999; Mir, Moscow, 1978).
- V. Sahni and A. Starobinsky, *Int. J. Mod. Phys. D* **15**, 2105 (2006).
- O.V. Verkhodanov, in *Proceedings of the 27th Radioastron. Conference on Modern Radioastronomy* (IPARAN, S.-Peterburg, 1997), vol. 1, p. 322.
- Yu.P. Pskovskii, *Sov. Astron.*, **6**, 172 (1962)
- S. Iskudarian, Yu.N. Pariiskii, *Izvestia GAO v Pulkove* **24**, 175(1967)
- S. Rawlings and M.J. Jarvis, *Mon. Not. R. Astron. Soc.* **355**, L9 (2004).
- Yu Lu, Ting-Gui Wang, Xiao-Bo Dong, and Hong-Yan Zhou, *Mon. Not. R. Astron. Soc.* **1761**, 404 (2010); arXiv:1002.0632 [astro-ph] (2010).
- J.J. Condon, W.D. Cotton, E.W. Greisen, et al., *Astron. J.* **115**, 1693 (1998).
- O.V. Verkhodanov, B.L. Erukhimov, M.L. Monosov, et al., *Bull. Spec. Astrophys. Observ.* **36**, 132 (1993).
- O.V. Verkhodanov, *ASP Conf. Ser.* **125**, 46 (1997).